International Journal of Research in Engineering and Science (IJRES)
ISSN (Online): 2320-9364, ISSN (Print): 2320-9356
www.ijres.org Volume 5 Issue 5 ǁ May. 2017 ǁ PP. 62-72

Black Silicon Photovoltaics: Fabrication methods and properties

Mayank Joshi[1], Reeta Verma[2]
[1](UG Scholar, Department of Electronics & Communication Engineering, College of Technology/ G.B.P.U.A.T, Pantnagar, India)
[2](Assistant Professor, Department of Electronics and Communication Engineering, College of Technology/ G.B.P.U.A.T, Pantnagar, India)

Abstract: *Black Silicon (BSi) is an interesting surface texture for solar cells because of its extremely low reflectance on a wide wavelength range and acceptance angle. This might lead to both an increase in efficiency and a reduction in the manufacturing costs of solar cells. The rise of BSi as a focus of study for its fundamental properties and potentially lucrative practical applications is shown by several recent results. A review of some common fabrication methods of black silicon, including metal-assisted chemical etching, reactive ion etching and laser irradiation process are discussed in the paper. Their resulting morphologies and a quantitative analysis of the optoelectronic properties are also presented and discussed. The utilization of BSi as an anti-reflection coating in solar cells is then critically examined and appraised. This review paper will serve as a useful introduction to this neoteric material and its properties and provide a general overview of recent progress in research currently being undertaken for renewable energy applications.*

Keywords: *Absorptance, Antireflection Coating (ARC), Black silicon, Nanostructures, Quantum efficiency*

I. Introduction

Black Silicon (BSi) as the name suggests- absorbs all the photons incidental on the surface and therefore appears black to the naked eye. The silicon surface is covered by a micro or nano structure layer. These structures effectively suppress the reflection and enhances the scattering and absorption of light. Reduction of reflection is a major criterion for the design of efficient solar cells. Such black silicon surfaces have a tremendous potential for photovoltaic applications. A common solution to minimize the reflection is an antireflection coating (ARC) applied on the front surface of a solar cell to suppress sunlight reflection [1]. However, simple ARC's based on quarter-wave-length layers perform well in a limited spectral range and for a certain angle of light incidence only. Black Silicon possesses near-zero reflection over a broad range of incident angles with features smaller than the wavelength of light, which eliminates the need for conventional vacuum-deposited ARC. When the size of surface features equals or exceeds the wavelength of the incident light, nano and microstructures also provide beneficial light trapping that increases the effective path length in the silicon [2]. BSi exhibits many attractive properties, such as low reflectance, a large chemically active surface area, and a high luminescence efficiency when surface feature sizes are reduced to a few nanometers. Over the past 15 years, many new BSi fabrication techniques have emerged and matured. At present, the methods of fabricating black silicon include a femtosecond (fs-) laser, metal-assisted wet etching, electrochemical etching, stain etching, plasma immersion ion implantation and reactive ion etching (RIE). Important design knowledge of BSi solar cells has been gained and a number of innovative solar cell architectures have been developed with a strong potential to further advance the power conversion efficiency of silicon solar cells at a decreasing cost [3]-[7]. In this paper, we provide a compendious review on the progress of BSi research, fabrication techniques and properties. The paper is organized as follows: first, different BSi fabrication techniques are introduced, with a brief review of the work done by different research groups. Then the optical and electrical properties of Black Silicon are examined.

II. Fabrication Techniques

Many BSi fabrication techniques have been developed over past decades. In this section, the major techniques are reviewed. Electrochemical HF etching, stain etching, metal-assisted chemical etching, reactive ion etching and laser irradiation have been well established and thoroughly reviewed by Xiaogang Liu *et al.* [8].

2.1 Laser Irradiation

Surface pattern formation upon laser irradiation with pulsed lasers has been first observed in the 1960s. Later the effect was also found for femtosecond laser pulses [9]. By irradiating a Silicon wafer with a fs- laser in SF_6, conical silicon spikes up to 50um high with a base area of 6x10 um2 were produced. Laser treatment in a SF_6 environment introduces sulphur atoms (1 atom %) and structural defects into the Si lattice of the final

product, thus creating more absorbing states in the sub-band gap region of Silicon. Due to minimization of surface reflection and introduction of sulphur atoms, an absorption efficiency of 90% has been observed, compared to an untreated silicon surface with absorption efficiency of merely 60% [10]-[12]. Furthermore, many parameters can be tuned to optimize the black silicon morphology and performance, such as laser polarization, spot size, power density, shot number, scanning parameter, and ambient environment. Laser power mainly determines the ablation and silicon volatilization rate and the pulse number controls the interaction time of laser and silicon substrate [13]-[15].

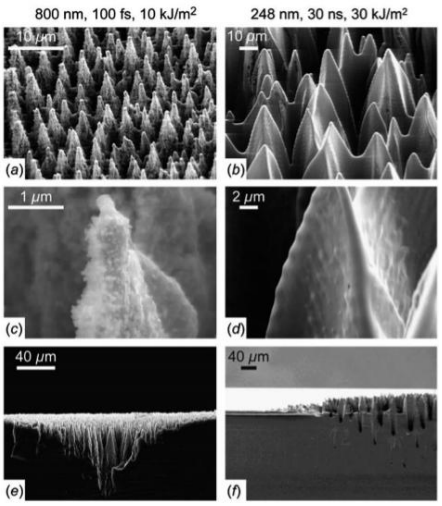

Fig. 1 SEM images of laser-treated silicon surfaces in a SF_6 environment with [(a), (c) and (e)] fs-laser, and [(b), (d) and (e) ns-laser. (e) and (f) show the side views of the snapped samples. [12]

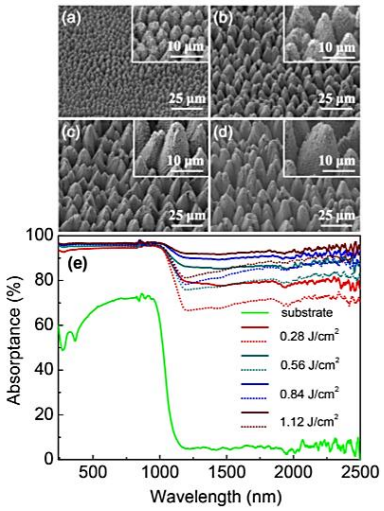

Fig. 2 (a)~(d) SEM images (tilt 45°) of phosphorus doped black silicon fabricated at different laser fluences: (a) 0.28, (b) 0.56, (c) 0.84, and (d) 1.12 J/cm^2, scale bars are 25 μm for (a)~(d) and 10 μm for inserts; (e) The absorptance of crystalline silicon substrate and SPL1~SPL4 before annealing (solid lines) and after the annealing (dash dot lines). [18]

Tsing Hua Her *et al.* fabricated arrays of sharp conical spiked by repeatedly irradiating silicon surface with fs- laser pulse in SF_6 or CL_2. 500 laser pulses of 100 fs duration with 100 KJ/m2 fluence in 66.66KPa SF_6 or Cl_2 were used. <100> silicon wafer was first cleaned with trichloroethylene, rinsed in acetone and then rinsed in methanol. These wafers were mounted on a three-axis translation stage in a vacuum chamber. This chamber was backfilled with 500 Torr (or 66.66KPa) Cl_2, SF_6, N_2, or He. Thereafter, these samples were irradiated with 500uJ, 800nm pulses from a regeneratively amplified Ti: sapphire laser. The laser pulses were focused with a 0.1m focal length lens. Each spot on the sample surface was exposed to a run of 500 lasers pulses. It is interesting to note that the tips of the spikes produced by this method were capped by a 1.5um ball when SF_6 was used. In case of CL_2, sharp spikes were obtained. Blunt spikes were observed in the case of N_2 or He [16].
Mengyan Shen *et al.* used fs- laser irradiation on a silicon surface immersed in water to achieve high density arrays of nanopillars. A single crystalline silicon substrate was placed in a glass container filled with water, mounted on a three-axis translation stage. The sample was irradiated by a 1KHz train of 100 fs, 800nm laser pulses. These pulses were focused by a 0.25m focal length lens and travelled through 10nm of water before striking the surface. A charged coupled device was used to analyze the spatial profile of laser. An average irradiation of 200 laser pulses was achieved by translating the sample at a speed of 500um/s perpendicular to the laser beam. The formation of regular arrays of nanometer scale rods/pillars enhanced the optical absorptance and decreased the reflectance to a very low level [17].

Chun-Hao Li *et al.* created an annealing-insensitive black silicon with high absorption by fs- laser direct writing. Microstructures with sized ranging from 4 to 25um were formed on surface layer of silicon substrate. The optical properties of the samples were measured using a Shimadzu UV-3600 spectrophotometer. With the help of spectrophotometer, the total hemispherical (specular and diffuse) reflectance(R) and transmittance(T) of the samples were measured in the range of 0.25 to 2.5um in 2nm increment and absorptance(A=1-R-T) was calculated at each wavelength. It is exciting to note that the absorptance below the band gap increased from 78% to 96% as the laser fluence increased [18].

T. Sarnet *et al.* prepared different absorbing structures for photovoltaic cells with different nano-texturing, obtained by fs- laser under vacuum (10-5 mbar). The optical set-up used to deliver the laser beam is presented in the figure 3. To achieve a more uniform laser energy distribution, only the middle part of Gaussian laser beam was selected using a square mask of 2x2 mm2. Penguin like structures were observed instead of spikes shown in figure 4. This was due to absence of corrosive gas like SF_6, CL_2. These structures had a height of about 10um with spacing of 2 to 5um and a flat high absorbance (>90%) over a broadband(350-1000nm) and weighted reflectance of 9% [19].

Jing Yang *et al.* achieved an exceptional average reflectance of 0.8% with the combined effect of laser

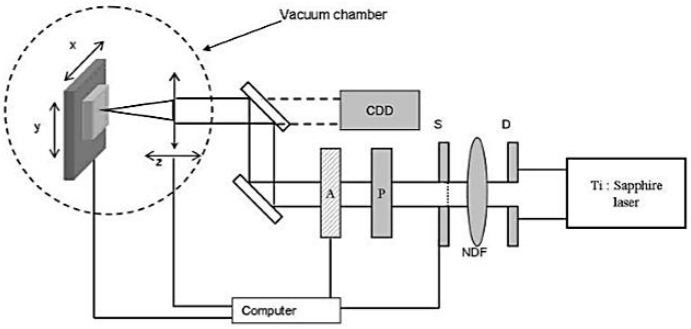

Fig. 3 Diagram of the fs- laser experimental setup [19].

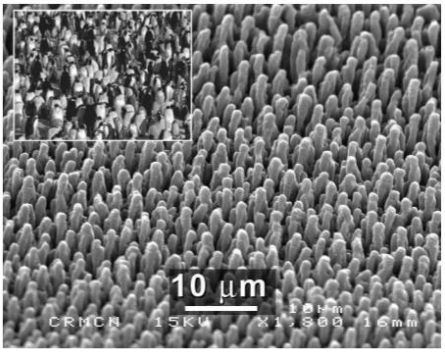

Fig. 4 SEM photo of penguin-like structures created by fs- laser [19].

irradiation and metal assisted chemical etching. Surface Plasmon Resonance(SPR) supported by metallic nanoparticles was used to suppress the reflection even more after laser irradiation. With the excitation of electromagnetic wave, metallic nanoparticles were used as anti-reflection surfaces because they excited localized SPR that increased the optical absorption by light trapping. The localized electromagnetic field around metallic nanoparticles was significantly enhanced at their resonant frequency. In general, we prefer Au or Ag but as the cost matter we may use Al and Cu [20].

The laser treatment process is relatively slow in comparison to other etching techniques, especially on an industrial scale, although its processing rate can be improved by increasing laser repetition rate, or raising the laser power/spot size. Also, laser induced material damage removal etching is required when a high-quality material is desired as in the case of photovoltaic applications.

2.2 Metal-Assisted Chemical Etching(MACE)

Zhipeng Huang *et al.* reviewed Metal Assisted Chemical etching(MACE) technique in detail. An illustration of the metal-assisted chemical etch process is shown in figure 5[21]. In the process given by Zhipeng Huang, a silicon substrate is partly covered by noble metal nanoparticles and immersed in a solution of HF and an oxidative agent, HNO_3. Usually, gold or silver are used since they can be deposited onto the surface under vacuum (via thermal evaporation, sputtering and electron beam evaporation) or in solution (i.e. via electro less deposition and electrodeposition). Electro less deposition method is much simpler and can be adopted when the requirement on silicon surface morphologies is less rigorous. Vacuum deposition offers a high degree fi control over the metal film morphology. During deposition, Au or Ag ions are added to HF-H_2O_2 solution. Upon attachment to silicon substrate noble metal ions acquire electrons from silicon valence band. Thus, electronic holes are injected into silicon just below metal. Subsequently, the holes diffuse to the silicon/electrolyte interface close to the particle. This results in tetravalent oxidation of silicon surface depending on local hole concentration. Then HF selectively etches the oxidized Silicon around the metal. As a result, the metal particles,

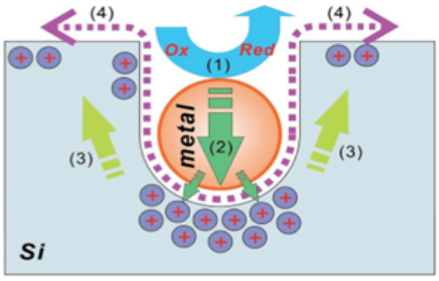

Fig. 5 An illustration of the metal-assisted chemical etch process: (1) the reduction of an oxidative agent (such as H_2O_2) catalyzed by a noble metal particle; (2) the injection of the holes generated during the reduction reaction, into the silicon substrate, with the highest hole concentration underneath the metal particle; (3) the migration of holes to silicon side walls and surfaces; and (4) the removal of oxidized silicon via HF [21].

"sink" into the silicon, generating pores in the silicon substrate or silicon wires. The depth of these pores is proportional to etching time. Once the desired surface structure is created, the metal nanoparticles are removed by another etchant, such as HNO_3. The size and shape of deposited metal particles largely determine the

morphologies of the etched surface, since the silicon underneath the metal is etched much faster. Different type of Black silicon layer, nanowires can be created by changing the surface coverage and distance between the metal particles.

Charlie *et al*. examined that in the case of Ag-assisted silicon chemical etching, a large variety of surface morphologies can be obtained by varying the etching solution composition. Mesopores, cone-shaped macropores, craters and eventually smooth surface was obtained as the ratio of HF/H_2O_2 varied from high to low as shown in figure 6. At high HF/H_2O_2 ratio, holes injection and Silicon dissolution occurred at the level of Ag nanoparticle only due to no formation of oxide at surface. At low HF/H_2O_2 ratio, the silicon surface is oxidized, the injected holes are homogeneously distributed and thus polished/smooth surface occurs. Cone shaped macropores occurs when injected holes diffuse away from Ag nanoparticles i.e. at moderate ratio of HF and H_2O_2[22].

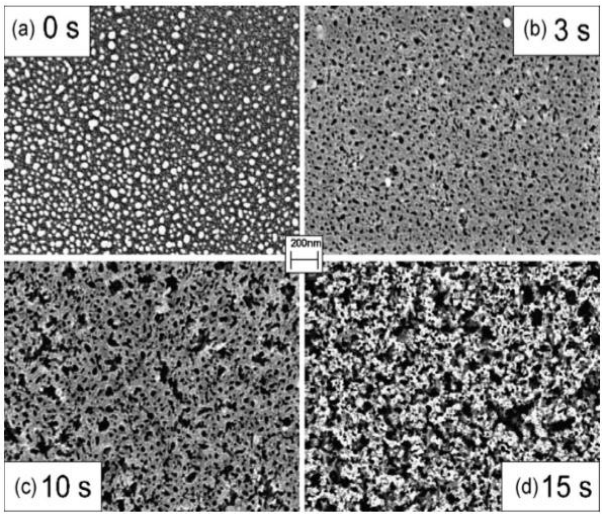

Fig. 6 SEM plan view images of a Ag loaded p-type <100> Si surface (a) and the porous Si layer produced by $HF-H_2O_2-H_2O$ etching (25/10/4) after 3s (b), 10s (c), and 15s (d) [22].

Nacera Megouda *et al.* performed Au-assisted electro less etching of p-type silicon substrate in HF/H_2O_2 solution at 50° Celsius. Si <100> substrate with different resistivity were used. The substrates were first cleaned by ultrasonication in acetone, ethanol and milli-Q water, followed by 3:1 concentrated H_2SO_4/30% H_2O for 20 minutes at 80° Celsius. Then these clean wafers were immersed in 50% HF aqueous solution for 1 minute at 25° Celsius to remove the native oxide. Gold films of 4 nm were deposited onto them. After rinsing the metal-deposited samples, they were immersed in an aqueous solution containing HF and H_2O_2 for etching at 50° Celsius for 10 minutes. Finally, it was concluded that the continuous Au film was broken into particles and then they sunk into Silicon wafer forming Nano or macro pores depending on size of Au particles. Figure 7 shows the cross-sectional view of SEM images of p-type Si [23].

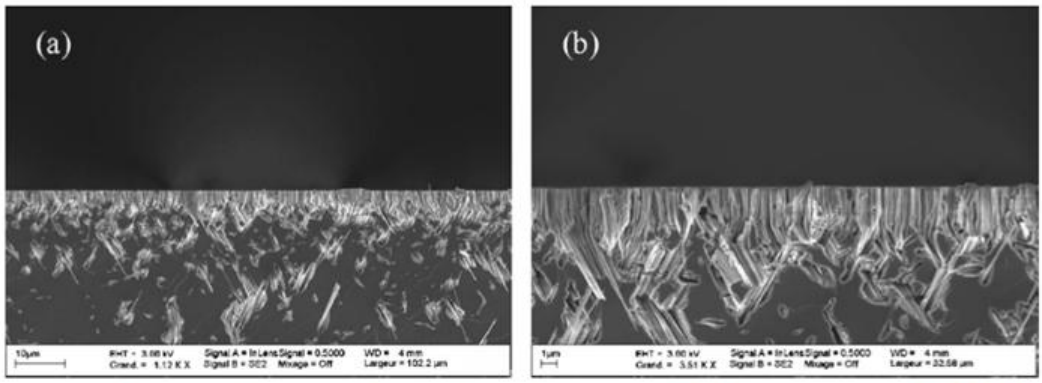

Fig. 7 Cross-sectional view SEM images of SiNWs formed on p-type Si (1 1 0) by etching in 26.35 M HF–0.9 M H_2O_2–H_2O solution at 50°C for 10 min(a). (b) is enlarged image. The Si resistivity is 1-10 Ω cm. [23]

Zengchao Zhao *et al*. characterized the performance of black silicon solar cells with various passivation films. A large black silicon wafer was prepared by Ag-nanoparticles assisted etching on pyramidal silicon wafer as shown in figure 8. It was observed that conversion efficiency of black silicon was highest for SiO_2/SiN_x:H stacks i.e. 17.1%. Whereas the conversion efficiency of BSi solar cell without passivation was 13.8%. Figure 9 depicts the IQE variation with the wavelength. The BSi with binary structure textured surface was produced by Ag-nanoparticle assisted etching, with 250 nm long nanowires and an average reflectance of about 3.42% [24].
In summary, MACE is a simple, fast, low cost process for fabricating a wide range of nanostructures with minimal hardware requirements.

2.3 **Reactive Ion Etching**

RIE forms needle like BSi surface, first proposed by Jansen *et al.* [25] in 1996 and thoroughly reviewed by Thomas Allen *et al*. in 2014. SF_6 and O_2 generate F* and O* radicals. F* radical causes etching, formation of volatile products like SiF_x. SiF_4 react with O* to form passivation layer of SiO_xF_y on a cooled Si substrate. This layer is partly removed by Ion bombardment and exposed Si is further etched. Etching reaction being exothermic in nature, reduces the chance of producing a new passivation layer since SiO_xF_y is prone to desorption upon heating. Side walls of Silicon columns do not experience much Ion bombardment; hence passivation layer is largely preserved, preventing further etching. This competition between etching and passivation mechanism leads to formation of random Si microstructure with very high aspect ratio in a self-masking fashion [26].

Yoo *et al*. designed a Multi-cathode RIE setup, making use of Hollow cathode effect. Number of cathodes are placed in parallel, allowing multiple wafers to be processed simultaneously, electrons are trapped between parallel oriented cathode and provide a high-density plasma. High density plasma causes higher etch rate, also characterized by its low voltage which ensures less ion induced wafer damage. Also, possible to

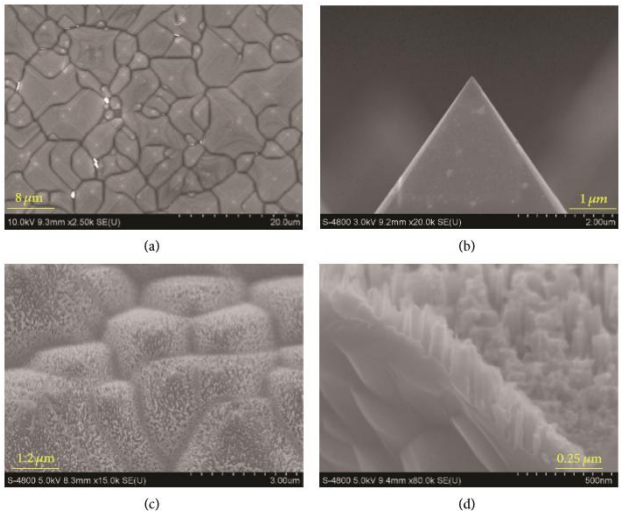

Fig. 8 SEM images of top view (a) and cross-sectional view (b) of pyramidal textured Si. SEM images of top view (c) and cross-sectional view (d) of as-etched binary structure textured BSi. [24]

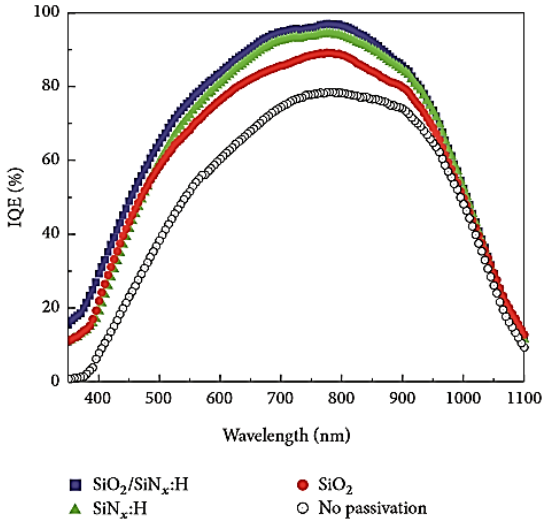

Fig. 9 Internal quantum efficiency (IQE) spectra of the BSi solar cell and BSi solar cells with SiO_2, SiN_x:H, and SiO_2/SiN_x:H stacks passivation films. [24]

replace or change the composition of reaction gases, SF_6/O_2[27].
Murias *et al*. added CH_4 into SF_6/O_2 to enhance micro-masking effect, due to formation of polymer on silicon. This RIE produced a high density of pyramid like structure, with average reflection of 4% in 400-700 nm region [28].

Lee et al. used Cl_2 as reactive gas instead of SF_6/O_2. It offers a lower etching rate but much easier to manager. It is claimed that in this system the in-situ surface damage removal could be realized by properly adjusting the plasma power density and gas composition. Cl_2 can also be added into SF_6/O_2 to enlarge gas composition [29]. Fuyun zhu *et al.* used a three-step model for modelling and simulation of Black silicon formation in DRIE process. The model divided the plasma etching into plasma layer, sheath layer and sample surface layer. Simultaneously, it combined quantum mechanics, sheath dynamics and diffusion theory together and predicted the probability distribution of etching particles. OpenDX was used to obtain the simulated morphologies by rendering them [30].

Daeyoung Kong *et al*. changed the nanocolumn structure of silicon on the micrometer pyramidal structure by Reactive Ion Etching texturing. A p-type <100> Silicon wafer was used upon which RIE texturing was performed in a plasma etching system with metal mesh (mesh size of about 100um). Finally, it was observed that silicon surface was covered with nanocolumn on the micropyramid structure, having diameters from 30 to 100nm and depth of about 300nm with average surface reflectance of about 2% was achieved. Figure 10 shows the variation of reflectance in accordance with the wavelength and schematic diagram of the RIE system in shown in figure 11 [31].

G. Kumaravelu *et al.* fabricated three different structures using RIE and compared them for surface

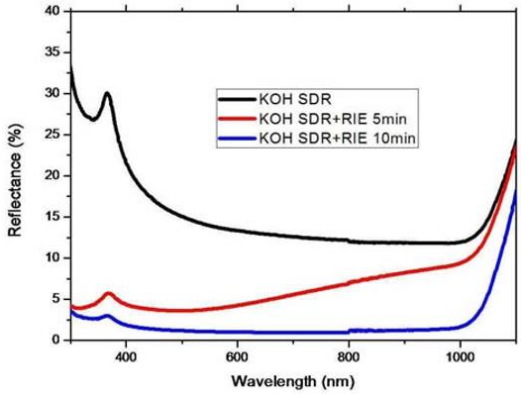

Fig. 10 Reflectance of crystalline RIE texturing processed for 5, 10 min and KOH SDR [31].

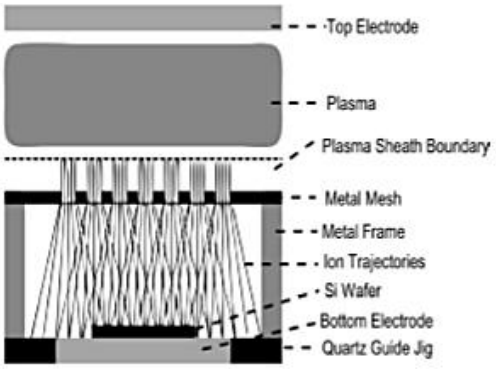

Fig. 11 Schematic diagram of the RIE system [31].

texturing. Column structure, hole structure, mask-less etched structure with reflectance of less than 0.4%, 6.8% and 1.4% respectively at wavelengths from 400 to 1000nm was observed. Most importantly, this crystal orientation-independent texturing could be used both for monocrystalline and multicrystalline solar cells without introducing significant damage as evident from Sub-micron channeling contrast microscopy [32].

Ye Jiang and co-workers created black silicon on a pyramid silicon surface via reactive ion etching through a Cu miromask formed by sputtering an annealing process. This technique avoids the use of O_2 which is beneficial because there is always a possibility of oxygen plasma damaging the silicon surface. A lowest reflectance of 6.2% was achieved by sputtering the samples for 240s, together with post-annealing and the RIE process [33]. Li Zhang *et al.* introduced a novel one step method to fabricate black silicon with varying scale. It is based on a commercial STS DRIE system with a phase delay producer. <100> oriented p-type Silicon wafer were cleaned, rinsed in deionized water and dried by nitrogen. Then using lithography masks, different scale etching windows were formed on surface of Si wafer. After that, a standard Bosch DRIE process, with SF_6/O_2

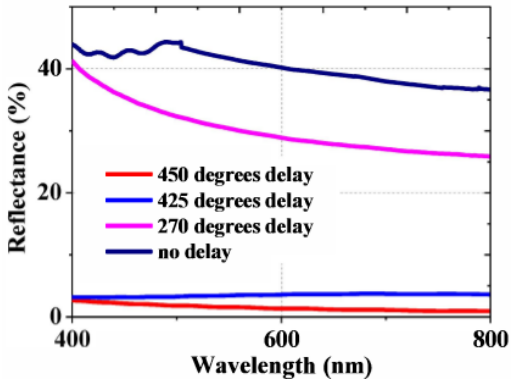

Fig. 12 The reflectance of the samples with different phase differences. [34]

etch gas and C_4F_8 passivation gas were conducted at room temperature. Nano- to microscale structures were fabricated by varying the trigger delays from 0 to 450°. The reflectance of black silicon was measured and the results are plotted in figure 12 [34].

III. Properties

3.1 Optical Properties

With the combined effect of anti-reflection coatings and surface texturing, the front surface reflection is reduced in thick wafer based solar cells. Traditionally, wet etching is used to develop textures on silicon solar cells because of its low cost, good uniformity across large areas, and high etching rate. Alkaline wet etching is mostly used to form pyramid structures that are 10-15 um deep for light scattering and anti-reflection applications, resulting in a reflectance of about 15% without anti-reflection coating. When a quarter-wavelength anti-reflection coating (SiO2, SiNx) is added, reflectance is further suppressed to 2%. The major drawback is that alkaline etching is anisotropic and forms undesirable steps along the boundaries in mc-Si wafer. By decreasing the thickness of solar wafers, material cost is reduced and requirements on wafer impurity levels and carrier diffusion lengths is relaxed. But as the wafer thickness decreases, it becomes difficult to undertake traditional wet etching. A solution to this problem is to use BSi. It helps to reduce reflectance in the following ways. First, reflectance is reduced as there is plenitudes of interactions of light with textured surface. Second, as the size of texture features is larger than the wavelength of visible light spectrum, the surface scattering is

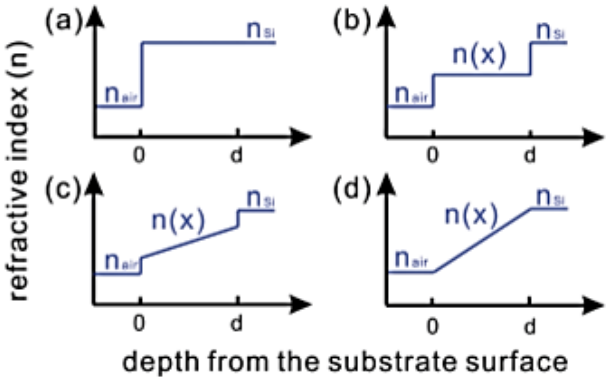

Fig. 13 Refractive index profiles from air to (a) a silicon wafer without any ARC; (b) a silicon wafer with a porous silicon layer of constant porosity; (c) and (d) silicon wafers with gradient porosities [41].

responsible for elongated light paths and an enhanced absorption. Third, a smooth refractive index transition from air to bulk silicon, via the nanostructured surface, results in an effectively graded-index anti-reflection coating which affords a strongly reduced reflectance. Refractive index profiles are shown in figure 14 [35]-[41]. When it comes to define the reflectance in mathematical equations, it is quite difficult because the optical constants for BSi change according to the morphology. Sita *et al*. defined an effective refractive index(n) and an effective extinction coefficient(k) based on phenomenological approach.

$$R = ((n_1 - n_2)^2 + k^2)/((n_1 + n_2)^2 + k^2) \quad (1)$$

$$T = \exp(-\alpha t) \quad (2)$$

$$\text{Absorption coefficient } \alpha = 4\pi k/\lambda \quad (3)$$

$$A = 1 - R - T \quad (4)$$

R, T, α, A, n, k are all functions of wavelength, λ

Here, medium 2 is air, n_2=1. The values of n and k are calculated from the R, T and A values obtained from the figure 15 and by using equations (1), (2), (3) and (4). This wavelength region corresponds to the energy band gap of silicon. Sita *et al*. further discovered that the absorptance of BSi significantly increased as the thickness was increased. The values of the absorptance corresponding to the different values of thickness is given in the Table 1 [42].

Table 1. Absorptance of Bsi at different thickness and wavelength [42]

Wavelength (um)	Thickness 1 um	Thickness 5 um	Thickness 10 um
0.5	0.557	0.978	0.994
1.0	0.428	0.931	0.984
1.5	0.444	0.933	0.976
2.0	0.421	0.919	0.979
2.45	0.446	0.919	0.972

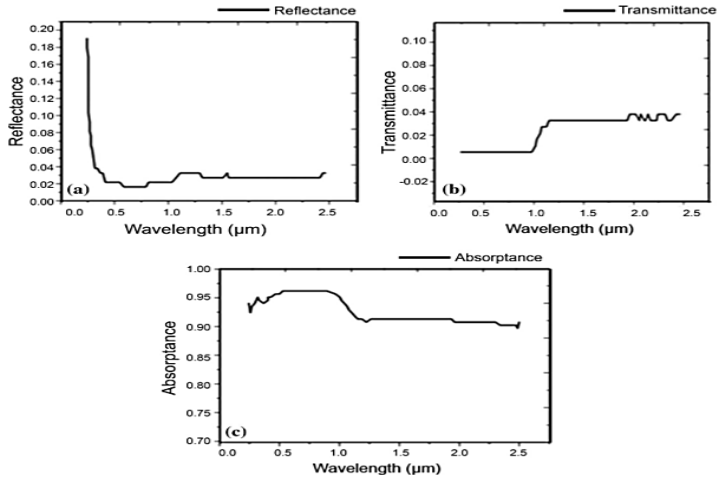

Fig .14 (a) Reflectance, (b) transmittance and (c) absorptance of BSi. [42]

Xin-Yue Yu *et al.* fabricated a co-doped black silicon with sulphur and nitrogen impurities by a fs- laser in a mixed atmosphere of N_2 and SF_6 and compared it with sulphur-doped black silicon. Xin-Yue Yu observed that the infrared absorption of co-doped BSi shows excellent thermal stability, indicating that the high absorption below the band-gap of silicon is insensitive to thermal annealing process. Moreover, the absorbance in the near infrared region of doped BSi showed a decreasing tendency with increasing N content in the mixed gas (for mol ratio of N_2: 0.25, 0.5 and 0.75) [43]. Furthermore, the polarization and angular dependence of BSi have been tested by Xie *et al.* and Huang *et al.* on samples fabricated via metal-assisted chemical etching and RIE respectively. Both types of samples demonstrated a low reflectance up to a large incident angle of about 80° [44]-[45].

1.1. Electrical Properties

Black silicon solar cells generally show low power conversion efficiencies. The highest efficiencies observed are 18.2% by Oh *et al*. [46] and 18.7% by P. Repo *et al*. [47] Many solar cells with different efficiencies and characteristics, fabricated by a variety of methods are listed in the Table 2.

Table 2. *J-V* parameters and efficiencies(eff.) of BSi fabricated through different methods

S/N	BSi fabrication method	Si type/size	V_{oc} (mV)	J_{sc} (mA cm^2)	FF (%)	Eff. (%)	Remarks	Ref.
1	Electrochemical etching	c-Si (CZ), 4 cm^2	579	28.8	76	12.7	No further passivation; selective emitter	48
2	Electrochemical etching	c-Si (FZ), 4 cm^2	603	30.4	78	14.3	No further passivation; selective emitter	49
3	Electrochemical etching	c-Si (FZ), 4 cm^2	601	31.3	78	14.6	No further passivation; micro-nano dual- scale surface texture; selective emitter	49
4	Stain etching	mc-Si, size not specified	569	25.5	68	9.6	No further passivation; selective emitter	50
5	Stain etching	mc-Si, 25 cm^2	609	29.1	79.7	14.1	No further passivation; selective emitter	49
6	Metal-assisted chemical etching	mc-Si, 243.36 cm^2	604	33.9	77.3	15.8	SiO_2/SiN_x stacked layer passivation	51
7	Metal-assisted chemical etching	c-Si, 243.36 cm^2	616	33.0	77.3	16.1	SiO2 passivation; micro-nano dual-scale surface texture	24
8	Metal-assisted chemical etching	mc-Si, 232.6 cm^2	624	36.1	76.2	16.4	SiO_2/SiN_x stacked layer passivation	52
9	Metal-assisted chemical etching	c-Si/243.36 cm^2	615	34.6	76.0	16.5	SiN_x passivation; micro-nano dual-scale surface texture	24
10	Metal-assisted chemical etching	c-Si (FZ), 4 cm^2	621	33.1	80.2	16.5	Al_2O_3/SiN_x stacked layer passivation; micro-nano dual scale surface texture	53
11	Metal-assisted chemical etching	c-Si (FZ), 1 cm^2	621	34.1	80.6	16.8	SiO2 passivation; NREL tested	54
12	Metal-assisted chemical etching	mc-Si, 243.36 cm^2	624	35.2	77.2	16.9	SiN_x passivation; selective emitter	55
13	Metal-assisted chemical etching	c-Si (FZ), size not specified	615	35.6	78.2	17.1	SiO_2 passivation; micro-nano dual-scale surface texture; NREL tested	56
14	Metal-assisted chemical etching	c-Si, 243.36 cm^2	623	34.6	77.8	17.1	SiO_2/SiN_x stacked layer passivation micro-nano dual-scale surface texture	24
15	Metal-assisted chemical etching	c-Si (CZ), 156.25 cm^2	623	35.5	79.3	17.5	SiN_x passivation; micro-nano dual-scale surface texture	57
16	Metal-assisted chemical etching	c-Si (CZ), 0.92 cm^2	598	41.3	75.1	18.2	Al_2O_3 passivation	58
17	Metal-assisted chemical etching	c-Si (FZ), 0.8081 cm^2	628	36.5	79.6	18.2	SiO_2 passivation; NREL tested	46
18	Metal-assisted chemical etching	c-Si, 243.36 cm^2	639	37.2	79.1	18.8	SiN_x passivation; micro-nano dual-scale surface texture	59
19	RIE	mc-Si, 100 cm^2	566	25.0	72	10.2	SiO_2 passivation	27
20	RIE	c-Si, 98 cm^2	564	28.6	73	11.7	SiO_2 passivation	27
21	RIE	c-Si (CZ), 156.25 cm^2	611	32.5	77	15.1	SiN_x passivation	60
22	RIE	mc-Si, 243.36 cm^2	614	33.8	78.6	16.3	No passivation details specified	61
23	RIE	c-Si (CZ), 156.25 cm^2	617	36.8	76	16.8	SiN_x passivation	62
24	RIE	mc-Si, 225 cm^2	621	36.2	76.2	17.1	SiN_x passivation for both front and rear sides	63
25	RIE	c-Si, 156.25 cm^2	623	35.4	78.2	17.2	SiN_x passivation; micro-nano dual-scale surface texture	64
26	RIE	mc-Si, 243.36 cm^2	632	35.7	77.9	17.6	SiN_x passivation; selective emitter	65
27	RIE	c-Si (FZ), 4 cm^2	632	39.2	75.8	18.7	n-Type solar cell; Al_2O_3 passivation for front side and PassDop passivation for the rear side	47
28	Laser treatment	c-Si (FZ), 1 cm^2	507	39.2	72	14.1	SiO_2/SiN_x stacked layer passivation	66
29	Laser treatment	c-Si (FZ), 1 cm^2	507	39.2	71.4	14.2	SiO_2/SiN_x stacked layer passivation	67
30	Laser treatment	c-Si (FZ), 7.3 cm^2	658	37.3	75.0	18.4	SiO_2 passivation for both front and rear sides; double-sided buried contact solar cells	68

Abbreviations used: open circuit voltage, Voc; short circuit current density, Jsc; fill factor, FF; efficiency, Eff.; CZ, Czochralski wafers; FZ, flow zone wafers; NREL, National Renewable Energy Laboratory

On the basis of Table 2, it is concluded that, the main and unfortunate reason for relatively poor performance of black silicon solar cells is its nanostructured surface. This can be attributed to the following: (i) The enlarged surface area of silicon has plenty of dangling bonds and trapping centers which play as effective recombination center [69] (ii) A heavier doping concentration leads to an increased Auger recombination [70]. (iii) Poor metal contacts on BSi [47].

The increased surface area and surface structured defects leads to a high increase in surface recombination. Also, the diffusion of dopants is much better in BSi than the planar surface, which is beneficial but also leads to a very doping concentration in BSi emitters and causes Auger recombination. Oh *et al.* [46] identified and separately measured the surface recombination and Auger recombination in BSi solar cells and concluded that while the Auger recombination is a dominating factor for carrier losses in high doping regions, the surface recombination is a dominating factor only in low doping regions. In regions with moderate doping concentration, both Auger and surface recombination mechanisms are important. Figure 16 shows that the current density was almost constant till 0.5 volts.

It is quite difficult for the metals to connect the gaps between nanostructures, which results in poor metal

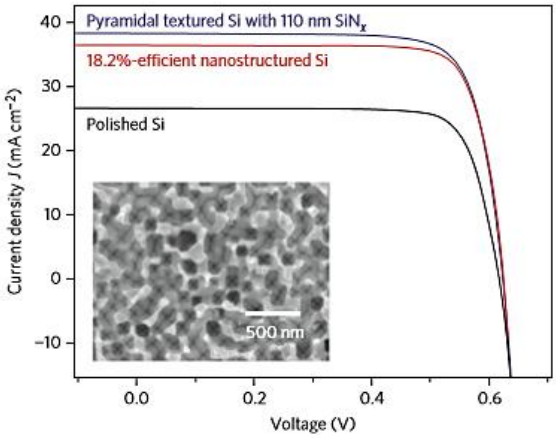

Fig. 15 J-V curves of 18.2%-efficient nanostructured black silicon, polished silicon and pyramidal-textured silicon with an SiNx anti-reflection coating under AM 1.5G illumination [46].

contacts. Moreover, many nanostructures have "self-cleaning" or super hydrophobic properties, which causes difficulties for screen printed metal contacts [7], [71]. Although the optical efficiency of BSi is quite high but still it is unable to compensate the electrical losses and therefore the overall power efficiency of Black silicon solar cells is low and the external quantum efficiency is poor in short wavelength region.

IV. Conclusion

In this paper, a comprehensive review of the different fabrication techniques of Black Silicon is discussed along with the resulting morphologies, optical and electrical properties of BSi. The methods studied are Laser irradiation process, Metal-assisted chemical etching and Reactive ion etching (RIE). It is observed that a wide range of surface morphologies can be achieved by varying the process parameters. For example, in laser irradiation process, by varying the laser polarization, spot size, power density, shot number, scanning parameter and ambient environment the black silicon morphologies and performance can be optimized. Similarly, it was observed in metal-assisted chemical etching that vacuum deposition of metal over the surface of silicon offers a high degree of control whereas the electroless deposition is much simpler and can be adopted when the requirement on silicon morphologies is less rigorous. The black silicon exhibits an excellent optical performance but its overall power conversion efficiency is quite low. The increased surface area due to nanostructures increases surface recombination and the better diffusion of dopants due to increased surface area and structured defects causes high doping regions which leads to Auger recombination. Poor metal contacts also cause electrical losses. Although the electrical performance is quite poor but due to high optical performance there are future possibilities to improve the electrical properties of Black silicon along with maintaining its optical properties to make black silicon as a future material for solar cells.

References

[1] I. Transactions, O. N. Electron, and D. Vol, *"Optimized Antireflection Coatings for High-Efficiency Silicon Solar Cells," vol. 38, no. 8, 1991.*

[2] E. Garnett and P. Yang, *"Light trapping in silicon nanowire solar cells," Nano Lett.*, vol. 10, no. 3, pp. 1082–1087, 2010.

[3] M. A. Tischler, R. T. Collins, J. H. Stathis, and J. C. Tsang, *"Luminescence degradation in porous silicon in porous,"* vol. 639, no. 1992, pp. 1–4, 2012.

[4] T. Her *et al.*, *"Microstructuring of silicon with femtosecond laser pulses Microstructuring of silicon with femtosecond laser pulses,"* vol. 1673, no. 1998, pp. 10–13, 2012.

[5] R. Li, S. Chuwongin, S. Wang, W. Zhou, "*Ag-Assisted Electrochemical Etching of Silicon for Antireflection in Large Area Crystalline Thin Film Photovoltaics ,"* vol. 2, no. c, pp. 2563–2565, 2011.

[6] H. F. W. Dekkers, F. Duerinckx, J. Szlufcik, and J. Nijs, *"Silicon surface texturing by reactive ion etching,*" *Opto-Electronics Review*, vol. 8, no. 4. pp. 311–316, 2000.

[7] Y. Xia, B. Liu, J. Liu, Z. Shen, and C. Li, *"A novel method to produce black silicon for solar cells," Sol. Energy*, vol. 85, no. 7, pp. 1574–1578, 2011.

[8] X. Liu, P. R. Coxon, M. Peters, B. Hoex, J. M. Cole, and D. J. Fray, *"Black silicon: fabrication methods, properties and solar energy applications," Energy Environ. Sci.*, vol. 7, no. 10, pp. 3223–3263, 2014.

[9] A. Y. Vorobyev and C. Guo, "*Applied Surface Science Direct creation of black silicon using femtosecond laser pulses*," *Appl. Surf. Sci.*, vol. 257, no. 16, pp. 7291–7294, 2011.

[10] E. Mazur and M. Shen, "*Femtosecond Laser-Induced Formation Of Submicrometer Spikes On A Semiconductor Substrate*," vol. 2138, pp. 1–14, 2008.

[11] C. Wu *et al.*, "*Near-unity below-band-gap absorption by microstructured silicon," Appl. Phys. Lett.*, vol. 78, no. 13, pp. 1850–1852, 2001.

[12] C. H. Crouch, "*2004_Crouch_Comparison of structure and properties of femtosecond and nanosecond laser-structured silicon," vol. 84, no. 11, pp. 11–16, 2004.*

[13] A. Medvid, P. Onufrijevs, G. Mozolevskis, E. Dauksta, and R. Rimsa, "*Two-stage model of nanocone formation on a surface of elementary semiconductors by laser radiation,*" pp. 1–6, 2012.

[14] A. V Kabashin, A. Pereira, D. Grojo, R. Torres, and M. Sentis, "*Nanofabrication with Pulsed Lasers*," pp. 454–463, 2010.

[15] W. G. Hawkins, J. G. Black, C. H. Griffiths, G. Hawkins, J. G. Black, and C. H. Griffiths, "*Growth of singlecrystal silicon islands on bulk fused silica by CO2 laser annealing Growth of single-crystal silicon islands on bulk fused silica by CO 2 laser annealing,*" vol. 319, no. 1982, pp. 2–5, 2001.

[16] T. Her *et al.*, "*Microstructuring of silicon with femtosecond laser pulses Microstructuring of silicon with femtosecond laser pulses,*" vol. 1673, no. 1998, pp. 10–13, 2012.

[17] M. Shen, J. E. Carey, C. H. Crouch, M. Kandyla, H. A. Stone, and E. Mazur, "*High-Density Regular Arrays of Nanometer-Scale Rods Formed on Silicon Surfaces via Femtosecond Laser Irradiation in Water 2008*," 2008.

[18] C. Li, J. Zhao, X. Yu, Q. Chen, J. Feng, and H. Sun, "*Fabrication of Black Silicon with Thermostable Infrared Absorption by Femtosecond Laser,"* vol. 655, no. c, pp. 1–6, 2016.

[19] T. Sarnet *et al.*, "*Femtosecond laser for black silicon and photovoltaic cells,*" vol. 6881, no. 33, 2008.

[20] J. Yang *et al.*, "*Design and fabrication of broadband ultralow reflectivity black Si surfaces by laser micro / nanoprocessing," J. Title*, vol. 3, no. 0, p. 0, 2014.

[21] Z. Huang, N. Geyer, P. Werner, J. De Boor, and U. Gösele, *"Metal-assisted chemical etching of silicon: A review*," *Adv. Mater.*, vol. 23, no. 2, pp. 285–308, 2011.

[22] C. Chartier, S. Bastide, and C. Lévy-Clément, "*Metal-assisted chemical etching of silicon in HF-H_2O_2*," *Electrochim. Acta*, vol. 53, no. 17, pp. 5509–5516, 2008.

[23] N. Megouda, T. Hadjersi, G. Piret, R. Boukherroub, and O. Elkechai, "*Au-assisted electroless etching of silicon in aqueous HF/H2O2 solution," Appl. Surf. Sci.*, vol. 255, no. 12, pp. 6210–6216, 2009.

[24] Z. Zhao, B. Zhang, P. Li, W. Guo, and A. Liu, *"Effective Passivation of Large Area Black Silicon Solar Cells by SiO_2 / SiNx : H Stacks,*" vol. 2014, 2014.

[25] H. Jansen, M. de Boer, R. Legtenberg, and M. Elwenspoek, "*The black silicon method: a universal method for determining the parameter setting of a fluorine-based reactive ion etcher in deep silicon trench etching with profile control," J. Micromechanics Microengineering*, vol. 5, no. 2, p. 115, 1995.

[26] T. Allen, J. Bullock, A. Cuevas, S. Baker-finch, and F. Karouta, "*Reactive Ion Etched Black Silicon Texturing : A Comparative Study*," pp. 562–566, 2014.

[27] J. S. Yoo *et al.*, "*Black silicon layer formation for application in solar cells*," *Sol. Energy Mater. Sol. Cells*, vol. 90, no. 18–19, pp. 3085–3093, 2006.

[28] D. Murias *et al.*, "*Black Silicon formation using dry etching for solar cells applications*," *Mater. Sci. Eng. B Solid-State Mater. Adv. Technol.*, vol. 177, no. 16, pp. 1509–1513, 2012.

[29] K. Lee, M. Ha, J. Hwan, and J. Jeong, "*Solar Energy Materials & Solar Cells Damage-free reactive ion etch for high-efficiency large-area multi-crystalline silicon solar cells," Sol. Energy Mater. Sol. Cells*, vol. 95, no. 1, pp. 66–68, 2011.

[30] F. Zhu, C. Wang, X. Zhang, X. Zhao, and H. Zhang, "*A three-step model of black silicon formation in deep reactive ion etching process,*" pp. 365–368, 2015.

[31] D. Kong, J. Oh, S. Jeon, B. Kim, C. Cho, J. Lee, "*Fabrication of black silicon by using RIE texturing process as metal mesh*," vol. 6, no. July, pp. 697–698, 2012.

[32] G. Kumaravelu, M. M. Alkaisi, A. Bittar, "surface texturing for silicon solar cells using reactive ion etching technique," pp. 258–261, 2002.

[33] Y. Jiang, H. Shen, Z. Yue, W. Wang, and J. Jin, "*Fabrication of black silicon via reactive ion etching through Cu micromask*," vol. 9, pp. 325–327, 2014.

[34] J. He, D. Zhao, and D. Zhang, "*A novel method to fabricate the black silicon for the solar cell*," no. 20, pp. 11–12.

[35] C. Lee, K. Tsujino, Y. Kanda, S. Ikeda, and M. Matsumura, "*Pore formation in silicon by wet etching using micrometre-sized metal particles as catalysts*," pp. 1015–1020, 2008.

[36] I. Zubel, "*Silicon anisotropic etching in alkaline solutions II On the influence of anisotropy on the smoothness of etched surfaces*," vol. 70, pp. 260–268, 1998.

[37] S. Chhajed *et al.*, "*Nanostructured multilayer graded-index antireflection coating for Si solar cells with broadband and omnidirectional characteristics Nanostructured multilayer graded-index antireflection coating for Si solar cells with broadband and omnidirectional characteristics*," vol. 251108, no. 2008, pp. 15–18, 2013.

[38] M. Steglich, T. Käsebier, M. Zilk, T. Pertsch, E. B. Kley, and A. Tünnermann, "*The structural and optical properties of black silicon by inductively coupled plasma reactive ion etching*," *J. Appl. Phys.*, vol. 116, no. 17, 2014.

[39] J. Shieh, C. Y. You, J. M. Liu, and C. C. Chiu, "*P-49 Improving optical and electrical properties of micropillar and black-Si solar cells by combining them into a superstructure,*" pp. 222–224.

[40] N. M. Ravindra and S. R. Marthi, S. Sekhri "*Modeling of Optical Properties of Black Silicon / Crystalline Silicon*," *Joutnal Sci. Ind. Metrol.*, vol. 1, no. 1, pp. 1–7, 2015.

[41] C. C. Striemer and P. M. Fauchet, "*Dynamic etching of silicon for broadband antireflection applications*," *Appl. Phys. Lett.*, vol. 81, no. 16, pp. 2980–2982, 2002.

[42] S. R. Marthi, S. Sekhri, and N. M. Ravindra, "*Optical Properties of Black Silicon: An Analysis*," *Jom*, vol. 67, no. 9, pp. 2154–2159, 2015.

[43] X.-Y. Yu, Z.-H. Lv, C.-H. Li, X. Han, and J.-H. Zhao, "*The Optical and Electrical Properties of co-doped Black Silicon Textured by a Femtosecond Laser and its Application to Infrared Light Sensing*," *IEEE Sens. J.*, vol. 16, no. 13, pp. 1–1, 2016.

[44] W. Q. Xie, J. I. Oh, and W. Z. Shen, "*Realization of effective light trapping and omnidirectional antireflection in smooth surface silicon nanowire arrays.*," *Nanotechnology*, vol. 22, no. 6, p. 65704, 2011.

[45] Y.-F. Huang *et al.*, "*Improved broadband and quasi-omnidirectional anti-reflection properties with biomimetic silicon nanostructures*," *Nat. Nanotechnol.*, vol. 2, no. 12, pp. 770–774, 2007.

[46] J. Oh, H.-C. Yuan, and H. M. Branz, "*An 18.2%-efficient black-silicon solar cell achieved through control of carrier recombination in nanostructures*," *Nat. Nanotechnol.*, vol. 7, no. 11, pp. 743–748, 2012.

[47] P. Repo *et al.*, "*N-type Black Silicon Solar Cells*," *Energy Procedia*, vol. 38, no. August 2015, pp. 866–871, 2013.

[48] L. Stalmans *et al.*, "*Porous Silicon in Crystalline Silicon Solar Cells : A Review and the Effect on the Internal Quantum Efficiency*," vol. 246, no. September 1997, pp. 233–246, 1998.

[49] S. E. Materials, S. Cells, J. Poortmans, B. View, and T. F. C. View, "*Multicrystalline silicon solar cells with porous silicon emitter Multicrystalline silicon solar cells with porous silicon emitter,"* no. May 2017, 2000.

[50] R. J. Mart, "*Antireflective porous-silicon coatings for multicrystalline solar cells : the effects of chemical etching and rapid thermal prcoessing*," vol. 657.

[51] *Y. Liu et al., "Nanostructure Formation and Passivation of Large-Area Black Silicon for Solar Cell Applications*," pp. 1–6, 2012.

[52] W. C. Hsu, Y. Lu, J. Chyan, and J. A. Yeh, "*High-Efficiency 6 Multicrystalline Black Solar Cells Based on Metal-Nanoparticle-Assisted Chemical Etching*," vol. 2012, 2012.

[53] Y. Liu, A. Das, Z. Lin, I. B. Cooper, A. Rohatgi, and C. P. Wong, *"Hierarchical robust textured structures for large scale self-cleaning black silicon solar cells*," *Nano Energy*, pp. 1–7, 2013.

[54] H. Yuan *et al.*, "*Efficient black silicon solar cell with a density-graded nanoporous surface : Optical properties , performance limitations , and design rules*," vol. 123501, no. 2009, 2012.

[55] Y. Wang, Y. P. Liu, T. Lai, H. L. Liang, Z. L. Li, F. M. Zhang, A. Kuznetsov, X. L. Du, "*Selective nano-emitter fabricated by silver assisted chemical etch-back for multicrystalline solar cells*," pp. 15483–15489, 2013.

[56] F. Toor *et al.*, "*Multi-scale surface texture to improve blue response of nanoporous black silicon solar cells Multi-scale surface texture to improve blue response of nanoporous black silicon solar cells*," vol. 103501, no. 2011, pp. 2011–2014, 2013.

[57] D. Z. Dimitrov and C. Du, "*Applied Surface Science Crystalline silicon solar cells with micro / nano texture*," *Appl. Surf. Sci.*, vol. 266, pp. 1–4, 2013.

[58] B. Tjahjono, J. Huang, W. Hsu, and M. Chen, "*Surface Passivation of E ffi cient Nanotextured Black Silicon Solar Cells Using Thermal Atomic Layer Deposition*," 2013.

[59] L. Yang *et al.*, "*Optimization of silicon pyramidal emitter by self-selective Ag-assisted chemical etching*," pp. 24458–24462, 2014.

[60] J. Yoo, G. Yu, and J. Yi, "*Black surface structures for crystalline silicon solar cells*," vol. 160, pp. 333–337, 2009.

[61] K. Lee, M. Ha, J. Hwan, and J. Jeong, "*Solar Energy Materials & Solar Cells Damage-free reactive ion etch for high-efficiency large-area multi-crystalline silicon solar cells*," *Sol. Energy Mater. Sol. Cells*, vol. 95, no. 1, pp. 66–68, 2011.

[62] J. Yoo, "*Reactive ion etching (RIE) technique for application in crystalline silicon solar cells*," *Sol. Energy*, vol. 84, no. 4, pp. 730–734, 2010.

[63] Y. Inomata, K. Fukui, and K. Shirasawa, "*Surface texturing of large area multicrystalline silicon solar cells using reactive ion etching method*," vol. 48, pp. 237–242, 1997.

[64] J. Liu, B. Liu, S. Liu, Z. Shen, C. Li, and Y. Xia, "*Surface & Coatings Technology A simple method to produce dual-scale silicon surfaces for solar cells*," *Surf. Coat. Technol.*, vol. 229, pp. 165–167, 2013.

[65] J. Shim *et al.*, "*17 . 6 % Conversion Efficiency Multicrystalline Silicon Solar Cells Using the Reactive Ion Etching with the Damage Removal Etching*," vol. 2012, 2012.

[66] V. V Iyengar, B. K. Nayak, and M. C. Gupta, "*Solar Energy Materials & Solar Cells Optical properties of silicon light trapping structures for photovoltaics*," *Sol. Energy Mater. Sol. Cells*, vol. 94, no. 12, pp. 2251–2257, 2010.

[67] B. K. Nayak, V. V Iyengar, and M. C. Gupta, "*Efficient light trapping in silicon solar cells by ultrafast-laser-induced self-assembled micro / nano structures*," no. January, pp. 631–639, 2011.

[68] H. S. Cells, "*Optical and Electrical*," no. January, pp. 225–235, 2006.

[69] S. Zhong *et al.*, "*Influence of the texturing structure on the properties of black silicon solar cell*," *Sol. Energy Mater. Sol. Cells*, vol. 108, pp. 200–204, 2013.

[70] E. Yablonovitch and T. Gmitter, "*Auger recombination in silicon at low carrier densities*," vol. 587, no. 1986, pp. 9–12, 2013.

[71] D. Qi *et al.*, "*Simple approach to wafer-scale self-cleaning antireflective silicon surfaces*," *Langmuir*, vol. 25, no. 14, pp. 7769–7772, 2009.